Materials Chemistry

Cite this: *J. Mater. Chem.*, 2012, **22**, 1341

www.rsc.org/materials

PAPER

Superhydrophobic supported Ag-NPs@ZnO-nanorods with photoactivity in the visible range†

Manuel Macias-Montero,[a] Ana Borras,*[a] Zineb Saghi,[b] Pablo Romero-Gomez,[a] Juan R. Sanchez-Valencia,[a] Juan C. Gonzalez,[a] Angel Barranco,[a] Paul Midgley,[b] Jose Cotrino[c] and Agustin R. Gonzalez-Elipe[a]

Received 23rd July 2011, Accepted 24th October 2011
DOI: 10.1039/c1jm13512k

In this article we present a new type of 1D nanostructures consisting of supported hollow ZnO nanorods (NRs) decorated with Ag nanoparticles (NPs). The 3D reconstruction by high-angle annular dark field scanning transmission electron microscopy (HAADF-STEM) electron tomography reveals that the Ag NPs are distributed along the hollow interior of the ZnO NRs. Supported and vertically aligned Ag-NPs@ZnO-NRs grow at low temperature (135 °C) by plasma enhanced chemical vapour deposition on heterostructured substrates fabricated by sputtered deposition of silver on flat surfaces of Si wafers, quartz slides or ITO. The growth mechanisms of these structures and their wetting behavior before and after visible light irradiation are critically discussed. The as prepared surfaces are superhydrophobic with water contact angles higher than 150°. These surfaces turn into superhydrophilic with water contact angles lower than 10° after prolonged irradiation under both visible and UV light. The evolution rate of the wetting angle and its dependence on the light characteristics are related to the nanostructure and the presence of silver embedded within the ZnO NRs.

Introduction

ZnO is a wide band-gap semiconductor which deserves the attention of many investigations because of its outstanding optical, electronic, acoustic or catalytic properties.[1] Particularly interesting in this field are the works devoted to the fabrication and the specific properties of ZnO 1D nanostructures.[1–9] Thus, ZnO materials formed by a high number of deposited nanowires have been demonstrated to present quite interesting properties for applications such as nanosensors, solar cells and photovoltaics, photonic devices, photocatalysis and, very recently, as active components in microfluidics.[6–11] On the other hand, the recent literature on 1D nanostructures of ZnO decorated with silver nanoparticles shows the high performance of these heterostructures in photocatalysis[12,13] and antibacterial applications.[14] One of the main roles of the 1D nanostructures in microfluidics relies on the formation of superhydrophobic surfaces, *i.e.* surfaces with water contact angles higher than 150°.[15–17] With the development of smart and laboratory-on-a-chip devices, a key characteristic of the surfaces is their reversible transformation from superhydrophobic into superhydrophilic (WCA close to 0°). Different approaches have been followed for this purpose as, for example, the use of electric field,[11,18–20] controlled heating treatments[21,22] or by irradiation with UV and recovery under VIS light.[10,23] The latter approach is advantageous when using 1D supported nanostructures since their manufacturing is usually compatible with the use of masks for patterning hydrophobic/hydrophilic surfaces, fast hydrophilic conversion, low energy cost and compatibility with a large number of substrates. In the present work we show a new type of ZnO based 1D nanostructures formed by supported hollow polycrystalline ZnO nanorods (NRs) decorated in their interior by silver nanoparticles (AgNPs). As will be discussed below, the surface formed by these Ag-NPs@ZnO-NRs, vertically aligned and high-density, deposited on any substrate surface, undergoes a superhydrophobic to superhydrophilic conversion under irradiation with visible light. As far as we know this is the first time that wetting photoactivity in the visible range is reported for ZnO 1D nanostructures. The application of plasma related techniques for the synthesis and process of nanomaterials has experienced an important development during the last few years.[24] The supported Ag-NPs@ZnO-NRs were fabricated by plasma enhanced chemical vapour deposition (PECVD) at low temperatures. A similar approach has been recently employed for the growth of randomly oriented core@shell Ag@TiO_2 nanofibers (NFs) by using metallic silver as the substrate.[25–27] Those nanostructures

[a]*Nanotechnology on Surfaces Laboratory, Materials Science Institute of Seville (ICMSE), CSIC-University of Seville, C/Americo Vespucio 49, 41092 Seville, Spain. E-mail: anaisabel.borras@icmse.csic.es*
[b]*Department of Materials Science and Metallurgy, University of Cambridge, Pembroke Street, CB2 3QZ, Cambridge, UK*
[c]*Department of Atomic and Nuclear Physics, University of Seville, Avda. Reina Mercedes s/n, 41012 Seville, Spain*
† Electronic supplementary information (ESI) available: Further TEM, SEM and STEM characterization; contact angle modelling and 3D reconstruction of the Ag-NPs@ZnO-NRs. See DOI: 10.1039/c1jm13512k

consisted of a core formed by a single crystalline thread of silver surrounded by a TiO_2 shell. Their formation was accounted for by a volcano-like mechanism where the main driving force is the release of the surface tension accumulated in a plasma oxidized silver substrate by the formation of silver threads. By using a slightly modified experimental approach in this work we have been able to deposit on any support vertically aligned Ag-NPs@ZnO-NRs which present a unique hollow nanostructure. To characterize this hollow structure and the distribution of silver within the NRs we have made use of the electron tomography (ET) in high-angle annular dark field scanning transmission electron microscopy (HAADF-STEM) mode. ET consists of reconstruction of 3D objects from a series of 2D projections acquired at different angles. The technique, originally developed for biological applications,[28] has been recently transferred to materials science and applied to various nanoscale structures, such as catalysts and semiconductor devices.[29,30] HAADF-STEM imaging mode was chosen here for two reasons: firstly, the HAADF-STEM signal is insensitive to diffraction contrast, and therefore provides the projection linearity needed for a reliable tomographic reconstruction; secondly, by choosing a large enough collection angle, the intensity in the HAADF-STEM images is approximately proportional to Z^2 (Z being the atomic number of the scattering atom).[31] HAADF-STEM mode is therefore ideal for imaging structures composed of elements with a large difference in Z, such as catalyst nanoparticles embedded in a light support.[32] We take advantage here of the high Z difference between silver ($Z_{Ag} = 47$) and ZnO ($Z_{Zn} = 30$, $Z_O = 8$) to highlight the 3D distribution of the particles within the wire.

The unique information supplied by this technique has provided a deep insight into the structure of the Ag-NPs@ZnO-NRs which, in turn, has allowed us to figure out their formation by plasma deposition at low temperatures. The proposed mechanism has similarities with the volcano-like process claimed by us to account for the formation of the Ag@TiO_2 NFs, but differs completely from the classical vapour–liquid–solid (VLS) mechanism generally responsible for the formation of 1D nanostructures in the presence of metal nanoparticles.[2–4,32–35] Although still subjected to some discussion, we have also related the light-induced wetting behaviour of the surfaces formed by the aligned Ag-NPs@ZnO-NRs with its internal nanostructure as determined by HAADS-STEM.

Results and discussion

Ag-NPs@ZnO-NR formation and 3D reconstruction

Fig. 1 shows several FESEM micrographs of the layer formed by Ag-NPs@ZnO-NRs grown on a Si(100) wafer previously decorated with silver particles deposited by DC sputtering (see the Experimental section and Fig. S1 in the ESI†). Fig. 1(a)–(d) show clearly that this layer consists of a continuous set of separated and vertically aligned NRs supported on the silicon substrate, with typical surface densities of $\sim 10^9$ NRs cm^{-2} (Fig. 1e). A statistical analysis of the images renders a mean diameter of ~40 nm and a height of ~900 nm for the NRs, *i.e.*, an aspect ratio of 20. Both the diameter and length of the NRs are controlled by the experimental parameters, particularly the deposition time. The number of NRs is determined by both the distribution of silver particles on the substrate and the precursor arrival rate to the surface. A thorough study of the factors controlling the formation of the Ag-NPs@ZnO-NRs is outside the scope of this communication and will be the subject of a forthcoming work. The crystal structure of these 1D heterostructures determined by GA-XRD for incident angles lower than 1° (Fig. 1f) consisted of the wurtzite structure of this oxide.[36] The pattern in Fig. 1(f) also shows the characteristic (111) and (200) reflections of the crystalline silver. Further characterization by HRTEM and SAED (Fig. 2) has shown the preferential growth of the ZnO following the [002] direction. Texture studies by XRD in Bragg–Brentano configuration might confirm that, however, the high porosity of the Ag@ZnO system hampers such a kind of characterization, resulting in a low intensity pattern predominantly dominated by the substrate peaks.

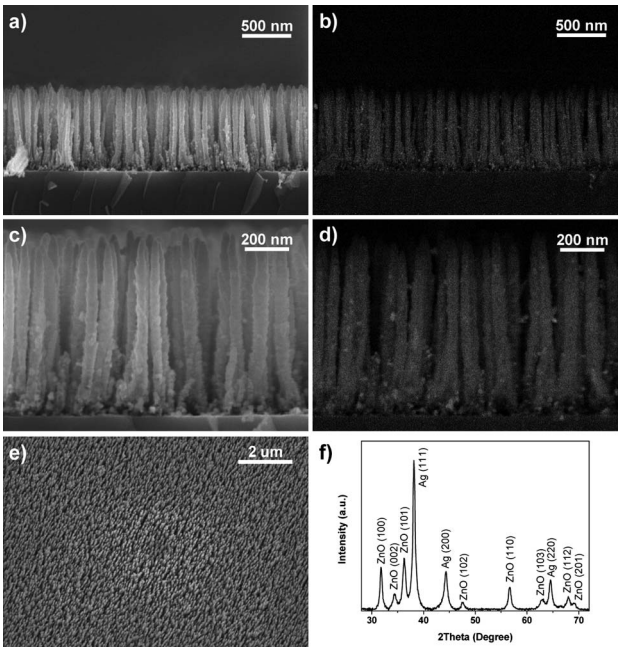

Fig. 1 Supported Ag-NPs@ZnO NRs grown by PECVD on a heterostructured Ag/Si(100) substrate. (a–d) Cross-section SEM micrographs recorded for secondary electrons (a and c) and for backscattered electrons (b and d); (e) normal view SEM image showing the high density of supported nanostructures prepared by this method; (f) GA-XRD pattern of the nanostructures.

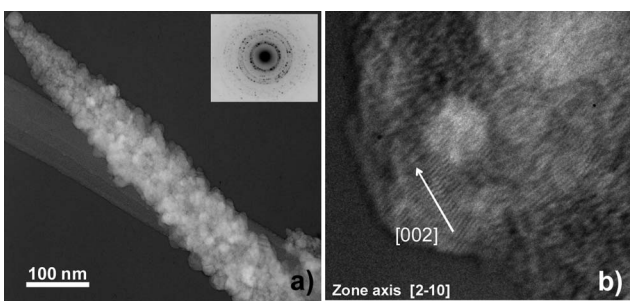

Fig. 2 (a) TEM micrograph and SAED pattern (inset) of a single Ag@ZnO-NW. (b) HRTEM micrograph of the ZnO nanocrystal showing the growth direction of the ZnO.

Fig. 1(b) and (d) obtained with backscattered electrons show the formation of silver particles along the NR length. Except for some particles that clearly appear on the surface of the NRs, traditional SEM and TEM characterizations (see Fig. 2a) do not reveal whether the Ag NPs are located in or outside the ZnO wire.

In consequence, the individual nanostructure and composition of the NRs were studied in detail by HAADF-STEM and EDX (Fig. 3). Two different NRs are shown in Fig. 3(a), both of them presenting a parabolic morphology and a highly porous microstructure. The comparison of the 1D nanostructures in Fig. 3(a) with those in Fig. 1(a)–(d) evidences that the NRs cross-section is not homogeneous along the NW length, their apex being thinner than their basis. Focusing on the longer NW in Fig. 3 (marked as NW#1 in the figure), it is also apparent that the bright spots in the HAADF-STEM micrograph correspond to Ag NPs of diameters comprised between 3 and 15 nm that are distributed along the ZnO nanostructure. The EDX spectra acquired on one of the bright spots and in the outer side of the wire (Fig. 3b) demonstrate that there is not any additional distribution of silver atoms on the nanowire, *i.e.* any possible silver doping the ZnO wire can be rejected.

To accurately describe the NRs morphology and further characterize their porous structure we performed the 3D reconstruction of the Ag-NPs@ZnO-NRs by electron tomography (Fig. 4). With this aim, HAADF-STEM images of the NRs in Fig. 3(a) were recorded at different tilt angles and subsequently aligned by cross-correlation before running the tomographic reconstruction using the iterative technique SIRT. The obtained 3D volume was visualized using the Amira software (see the Experimental section). Fig. 4 shows the main results obtained from this 3D reconstruction analysis of the NRs. In addition, Video S1† displays the full reconstruction of the NR, showing a hollow nanostructure where the ZnO arranges according to a radial conformation (see also Fig. 4(a) and (b)). Most of the Ag NPs are aligned in the interior of this hollow as it is shown in the cross-section slices in Fig. 4(b) and in the rendered representations of the NR (Fig. 4(c) and (d)). As far as we know this is the first time that such a heterostructure is obtained by a one-step vacuum deposition method. The characteristic arrangement of the Ag NPs along the hollow structure of the ZnO NW differentiates this 1D heterostructure from the core–shell Ag@TiO_2 NFs fabricated by a similar methodology on a silver metal substrate[25–27] and from the 1D nanostructures synthesized by VLS.[2–4,32–35] In the former case silver forms a continuous single crystalline thread, while in the latter the metal nanoparticles that act as catalyst in the 1D growth typically remain as a metal drop or particle on the top of the 1D nanostructure. In our case, we have observed that occasionally silver nanoparticles appear covering the Ag-NPs@ZnO-NRs, particularly at the earlier stages of the deposition (Fig. S2†). However, most of the silver NPs vanish inside the NRs after prolonged deposition times and therefore longer NR length. This evidence points to a certain permeability and porosity of the ZnO outer layer of the NRs.

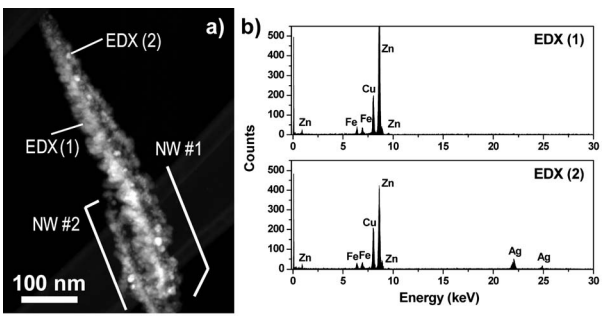

Fig. 3 STEM characterization of Ag-NPs@ZnO nanowires. (a) STEM micrograph of two Ag-NPs@ZnO NRs; (b) EDX spectra acquired at the spots marked in (a).

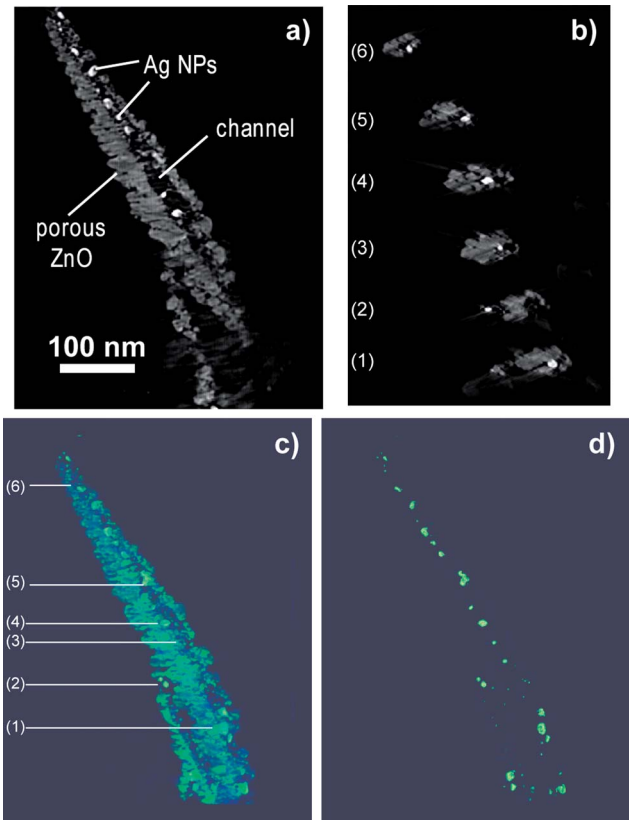

Fig. 4 3D reconstruction of the Ag-NPs@ZnO nanowires. (a) Vertical orthoslice through the reconstructed Ag-NPs@ZnO nanowire; the bright features correspond to the Ag NPs; (b) horizontal orthoslices along the Ag-NPs@ZnO nanowire length showing the position of the Ag NPs in the hollow ZnO structure; (c) voxel projection view of the reconstructed nanowire and (d) rendered reconstruction showing the position of the Ag NPs along the nanostructure. See the complete 3D reconstruction in Video S1 accessible in the ESI†.

Growth mechanism

Although additional experimental work is still required for establishing the growth mechanism of the Ag-NPs@ZnO-NRs, several pieces of experimental evidence can be highlighted as critical clues for their growth: (i) silver Huttig temperature and volume changes between silver and silver oxide: in a similar way to the formation of the Ag@TiO_2 NFs, the lower substrate temperature threshold required for the growth of the NRs is ~135 °C, very close to the Huttig temperature of silver at which atoms start moving and diffusing through structural defects.[26] As

previously shown, at this temperature and under oxidizing plasma conditions the silver behaves as a molten phase subjected to strong density changes because of the difference in specific volume between the silver and silver oxide phases. A suitable way to release such a surface stress is the formation of whiskers or segregated NPs. In this regard it is interesting that the mean diameter of the Ag-NPs inside the Ag-NPs@ZnO-NRs is much smaller than that of the corresponding silver particles on the substrate before the ZnO deposition (see also Fig. S1†). (ii) The parabolic shape of the NRs: the long conical morphology of the Ag-NPs@ZnO-NRs is a characteristic of the growth of 1D nanostructures by PECVD because the ions coming from the plasma phase are selectively focused first on the silver particles and then on the tips of the growing NRs.[37] Lateral inhomogeneities in the electrical field distribution associated with the Ag/ZnO growth must be a consequence of such behavior. (iii) High homogeneity in the NR length and diameter: even if the initial silver particle size distribution on the substrate is quite broad (Fig. S1†), the NR length and diameter are very homogeneous (*cf.* Fig. 1). These two features altogether with point (i) support the formation during the NR growth of a very mobile intermediate state of silver/silver oxide similar to a molten phase. A previous article by Xing *et al.*[38] has demonstrated the effective growth of ultra-thin ZnO nanobelts in the presence of silver. In that case the formation of the ZnO nanobelts was produced by transport and supersaturation of Zn vapor on a 2 nm Ag film at 470 °C. Xing *et al.* proposed a growth process involving both substantial precursor migration and effective mass redistribution, where Ag in its melting state may serve as a soft template to assist the vapor condensation and the subsequent nanobelt growth. Although in our case, a plasma assisted process, the number of factors contributing to the formation of the NRs increases the complexity of the growth mechanism, a similar role can be applied to the silver/silver oxide particles. Thus, supported on the experimental evidence, we tentatively propose a modified volcano mechanism for the formation of the Ag-NPs@ZnO-NRs. The main differences between the growth processes of Ag-NPs@ZnO-NRs and Ag@TiO_2 NFs are the different amounts of silver available for the formation of the core and likely a stronger influence of the ions coming from the plasma in the case of ZnO deposition. Under the present experimental conditions the amount of silver contained in the thin substrate layer is not enough to produce compact silver wires or threads. However, as it has been demonstrated by the 3D reconstruction, silver diffusion still occurs inside the nanowire, where silver NPs close to or at the tip of the NRs seem to favor their vertical growth by moving in its interior simultaneously to the supply of material from the plasma phase (*i.e.*, by "drilling" the hollow space inside the NW). The process occurs in such a way that ZnO grows as a porous shell while diffusing silver/silver oxide segregates from the substrate and moves through the interior of the NR. This surface diffusion is the result of the surface stress produced for the density changes between silver and the silver oxide (ρ_{Ag} = 9.32 g cm^{-3}, ρ_{Ag2O} = 7.14 g cm^{-3}) formed in a highly oxidized plasma environment.[26] Once the mobilization and oxidizing conditions (oxygen plasma and substrate temperature) are switched off the silver and/or the silver oxide fragments agglomerate and form the silver NPs that decorate the channel inside the 1D nanostructure.

Wetting behavior

A common approach for the fabrication of superhydrophobic coatings is the formation of highly rough surfaces of hydrophobic or partially hydrophobic materials, *i.e.* low surface energy materials.[39] Supported nanofiber arrangements have also been reported to depict a superhydrophobic behavior.[23,39,40] Similarly, the water contact angle (WCA) of a surface formed by a high density arrangement of Ag-NPs@ZnO-NRs (Fig. 1e) is higher than > 150° (*i.e.*, superhydrophobic, see insets in Fig. 5). Since the WCA of a flat ZnO reference thin film deposited under the same conditions on a Si(100) substrate is ~110°, we must relate the superhydrophobicity found for the NR surfaces to their highly rough nanostructure,[23,39,40] namely with the number of NRs per unit area, their length and diameter.[39,40]

The Wenzel and Cassie–Baxter[39,41] models try to correlate the actual WCAs measured on a rough surface with the angle that would be measured on an ideally flat surface of the same composition. We have applied the two models to our NR surfaces and found that while the Wenzel formula does not account properly for the experimental results, the Cassie–Baxter model permits to explain their superhydrophobic behavior by using a quite simple geometrical model to determine the roughness of the samples (see ESI†). The procedure implies the determination of the solid fraction ϕ_S in contact with the drop under the assumption that, at the interface, water is also in contact with the air confined between NRs (since the air–water WCA is 180°). According to this simple approximation the drop in contact with the surface follows the profile depicted in Scheme S1 in the ESI†, *i.e.* the water contact line with the NW does not reach the substrate. Although a more accurate model should take into account the shape of the water meniscus, from the simple calculations gathered in the ESI† we can conclude that the drop only wets the tips of the NRs and penetrates within the inter-NW space to a depth of the order of 300 nm.

Previous works have demonstrated that ZnO-NR surfaces become superhydrophilic (*i.e.* WCA < 10°) under UV irradiation because the surface of this material becomes photon activated and the water may then smoothly spread over the whole internal surface of the wire structure.[10] A similar behavior is depicted by the system Ag-NPs@ZnO-NRs where the conversion from a superhydrophobic to superhydrophilic state under UV illumination is completed after 8 min of irradiation under our

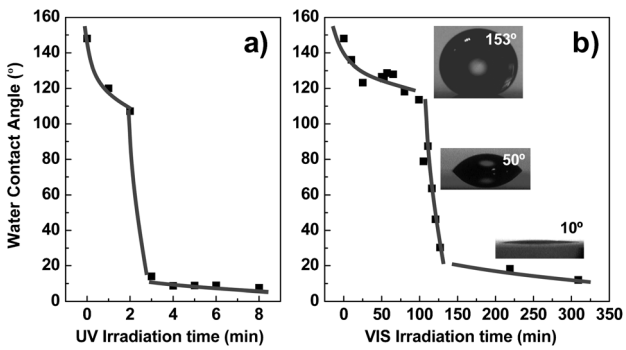

Fig. 5 Superhydrophobicity to superhydrophilicity conversion by light irradiation. Changes in the water contact angle induced by irradiation with UV (a) and VIS light (b), respectively.

experimental conditions (Fig. 4a). In agreement with ref. 10 and 42 the surface recovered its superhydrophobic character after keeping the samples in the dark (full recovery after 5 days). A close look at the WCA evolution in Fig. 5(a) evidences the existence of an inflexion point at around 2 min which denotes that a second mechanism has been triggered after irradiating for this time. A similar superhydrophobic–superhydrophilic conversion was found when this surface was irradiated with visible (VIS) light (*cf.* Fig. 5b). The WCA decreases under the VIS illumination until reaching a superhydrophilic state (WCA lower than 10°). Visible illumination is much less effective since a WCA < 10° is only reached after irradiating for ~150 min. However, this activation process permits the clear confirmation of the existence of a drastic change in the wetting transformation process that now is triggered after irradiating for approximately 80 min. Visible light activation of ZnO can be surprising since this material is a band gap semiconductor which requires UV photons ($E \approx 3.2$ eV) for excitation. However, partial hydrophobic to hydrophilic conversion has been found in ZnO and other semiconducting oxides when irradiated with VIS light in a process that has been associated with the surface excitation of surface defect states in the gap.[42,43] On the other hand, it is already established that the deposition of noble metals on semiconductors promotes an enhancement in their photocatalytic activity by indirect influence on the interfacial charge transfer process.[12,13,44,45] In these cases, silver can act as electron scavenger and charge store. Enhanced photocatalytic activity has been reported previously for Ag/ZnO systems comprising ZnO 1D nanostructures decorated with silver fabricated by different methods.[12,13,44] Wang *et al.*[12] have concluded that the presence of Ag nanoparticles increases the hydroxyl contents at the surface of ZnO microspheres formed by ZnO nanorods. Pillai *et al.*[44] have also shown the enhanced photocatalytic activity for a critical amount of silver in ZnO nanoparticles in the degradation of rhodamine 6G. Those experiments further demonstrated that the presence of silver facilitated the interfacial charge transfer processes in such a way to utilize the conduction band electrons for enhancing the photocatalytic activity. In particular, superoxides and OH radicals were formed by the Ag discharged of the stored electrons into the solution where they reacted with the dissolved oxygen. Similar excitation processes can be invoked here with the peculiarity that they lead to a complete superhydrophilic transformation, probably promoted by the very particular architecture of the polycrystalline hollow Ag-NPs@ZnO-NRs. The 3D tomographic reconstruction performed by HAADF-STEM has shown that the ZnO shell presents a highly porous structure (Fig. 4). We can expect that the ZnO close to the Ag particles behaves as a superhydrophilic surface because of the enhanced hydroxyl enrichment under irradiation. It is also important to remark that for both UV and VIS illumination the inflexion point for the curves in Fig. 5 is *ca.* 110°. These results might indicate that the porous polycrystalline surface of the NRs becomes superhydrophilic by gradual conversion of different crystal planes in a similar way to for the TiO_2 surface in the amphiphilic model.[41,46] Once all the different crystal planes are converted the water contact angle would change drastically by combination with the photocatalytic enhancement because of the presence of Ag. Under such conditions the system would partially behave as a sponge, implying that the Cassie–Baxter assumptions do not apply any more.

Experimental section

Sample preparation

Heterostructured Ag substrates are fabricated by DC sputtering from a 99.99% purity Ag wire in argon (in the range between 1.5 and 2 mbar) at room temperature. Typical substrates were Si (100) wafers, fused silica, quartz slides and ITO. The heterostructured substrates were located in a PECVD reactor for the deposition of ZnO. The PECVD system consists of a high vacuum chamber attached to a microwave electron–cyclotron-resonance (MW-ECR) SLAN I plasma source according to a downstream configuration, *i.e.* out of the plasma discharge. The ZnO precursor, diethyl zinc (DEZ), was purchased from Aldrich. It was dosed in the vacuum chamber through a mass flow controller and distributed between the plasma discharge and the substrate surface by a shower-like dispenser. The Ag-NPs@ZnO-NRs are formed under oxygen plasma at 4×10^{-3} Torr operated at 400 W and a substrate temperature of 135 °C. In order to improve the density and homogeneity of the Ag-NPs@ZnO-NRs, the Ag substrates are first pre-treated in pure oxygen plasma (4×10^{-3} Torr) at 135 °C for 1 hour.

Sample characterization

Cross-section and normal view SEM images were acquired in a Hitachi S4800 microscope. GAXRD studies were performed in an X'Pert Pro from PANalytical for X-ray angles <1°. For the TEM characterization Ag-NPs@ZnO nanowires were removed from the substrates by scratching and dispersion in ethanol and then "fished" in a holey carbon grid (from Plano). Bright field TEM was carried out in a CM200 from Phillips. HAADF-STEM electron tomography was performed on a FEI Tecnai F20 field-emission gun transmission electron microscope operated at 200 kV. Data collection was carried out by tilting the specimen about a single axis from −64° to +62° with a 2° increment, using a Fischione ultrahigh-tilt tomography holder, and acquiring the images with the FEI software package Xplore3D. The tilt series was then exported to the FEI software Inspect3D for the cross-correlation alignment and the tomographic reconstruction using the iterative routine SIRT. Slice viewing and surface rendering after a global thresholding were undertaken using Amira software. Static water contact angle measurements were carried out by the Young method with droplet volumes of ~5 μl with a CAM100 instrument (KSV Instruments Ltd., Finland). The samples were irradiated with and without a visible filter with a Xe lamp. An additional infrared filter was utilized in order to prevent the heating of the samples. The photon intensity at the position of the samples was 2 W cm^{-2} for the UV irradiation experiments (also including the VIS light photons) and 1.6 W cm^{-2} when operated with the visible filter.

Conclusions

In summary, herein we have reported on the PECVD synthesis of a high density film formed by separated Ag-NPs@ZnO-NRs. The characterization of these NRs by the HAADF-STEM

tomographic reconstruction has demonstrated their unique morphology consisting of a hollow ZnO structure in whose interior are distributed Ag NPs of different sizes. This morphology has been discussed in terms of a growth model that would be a modification of the so-called "Volcano"-like mechanism proposed previously to account for the formation of $Ag@TiO_2$ nanofibers. We have also investigated the wetting behaviour of the Ag-NPs@ZnO-NR surfaces and found that the surface formed by a high density of NRs presents WCA > 150°. An outstanding property of these surfaces is the possibility to change its WCA from a superhydrophobic to a superhydrophilic state by using VIS light, a characteristic that we attribute to the particular morphology of the NRs and to the incorporation of Ag NPs in its interior. We expect these results to be of great interest in microfluidic and photocatalysis in the VIS range.

Acknowledgements

This work was funded by the EU (project NMP3-CT-2006-032583), the Spanish MICINN (projects MAT2010-21228, MAT2010-18447 and Consolider CSD2008-00023) and JUNTA de Andalucía (projects P09-TEP-5283, CTS-5189). JCG thanks the Spanish Scientific Research Council (CSIC) for his JAE-Doc contract (2009-2012) at the ICMSE-CSIC-US. ZS and PAM acknowledge financial support from the European Union under the Framework 6 program under a contract for an Integrated Infrastructure Initiative, Reference 026019 ESTEEM.

Notes and references

1 Z. L. Wang, *Mater. Sci. Eng., R*, 2009, **64**, 33.
2 Y. Tak, K. Yong and C. Park, *J. Electrochem. Soc.*, 2005, **152**, G794.
3 M. Haupt, A. Ladenburger, R. Sauer, K. Thonke, R. Glass, W. Roos, J. P. Spatz, H. Rauscher, S. Riethmuller and M. Moller, *J. Appl. Phys.*, 2003, **93**, 6252.
4 D. Ito, M. L. Jespersen and J. E. Hutchison, *ACS Nano*, 2008, **2**, 2001.
5 J. Elias, R. Tena-Zaera, G.-Y. Wang and C. Levy-Clement, *Chem. Mater.*, 2008, **20**, 6633.
6 W.-Y. Wu, J.-M. Ting and P.-J. Huang, *Nanoscale Res. Lett.*, 2009, **4**, 513.
7 M. H. Huang, S. Mao, H. Feick, H. Yan, Y. Wu, H. Kind, E. Weber, R. Russo and P. Yang, *Science*, 2001, **292**, 1897.
8 M. Law, L. E. Greene, J. C. Johnson, R. Saykally and P. Yang, *Nat. Mater.*, 2005, **4**, 455.
9 H. Koga, T. Kitaoka and H. Wariishi, *J. Mater. Chem.*, 2009, **19**, 2135.
10 X. Feng, L. Feng, M. Jin, J. Zhai, L. Jiang and D. Zhu, *J. Am. Chem. Soc.*, 2004, **126**, 62.
11 J. L. Campbell, M. Breedon, K. Latham and K. Kalantar-Zadeh, *Langmuir*, 2008, **24**, 5091.
12 W. Lu, S. Gao and J. Wang, *J. Phys. Chem. C*, 2008, **112**, 16792.
13 D. Lin, H. Wu, R. Zhang and W. Pan, *Chem. Mater.*, 2009, **21**, 3479.
14 H. Koga, T. Kitaoka and H. Wariishi, *J. Mater. Chem.*, 2009, **19**, 2135.
15 A. Marmur, *Langmuir*, 2009, **25**, 1277.
16 M. Ma, R. M. Hill and G. C. Rutledge, *J. Adhes. Sci. Technol.*, 2008, **22**, 1799.
17 J. Yuan, X. Liu, O. Akbulut, J. Hu, S. L. Suib, J. Kong and F. Stellacci, *Nat. Nanotechnol.*, 2008, **3**, 332.
18 B. Kakade, R. Mehta, A. Durge, S. Kulkarni and V. Pillai, *Nano Lett.*, 2008, **8**, 2693.
19 N. Verplanck, E. Galopin, J. C. Camart, V. Thomy, Y. Coffinier and R. Boukherroub, *Nano Lett.*, 2007, **7**, 813.
20 T. N. Krupenkin, J. A. Taylor, T. M. Schneider and S. Yang, *Langmuir*, 2004, **20**, 3824.
21 H. Z. Wang, Z. P. Huang, Q. J. Cai, K. Kulkarni, C.-L. Chen, D. Carnahan and Z. F. Ren, *Carbon*, 2010, **48**, 868.
22 J. Yang, Z. Zhang, X. Men, X. Xu and X. Zhu, *Carbon*, 2011, **49**, 19–23.
23 A. Borras, A. Barranco and A. R. Gonzalez-Elipe, *Langmuir*, 2008, **24**, 8021.
24 K. Ostrikov, U. Cvelbar and A. B. Murphy, *J. Phys. D: Appl. Phys.*, 2011, **44**, 174001.
25 A. Borras, A. Barranco, F. Yubero and A. R. Gonzalez-Elipe, *Nanotechnology*, 2006, **17**, 3518.
26 A. Borras, A. Barranco, J. P. Espinos, J. Cotrino, J. P. Holgado and A. R. Gonzalez-Elipe, *Plasma Processes Polym.*, 2007, **4**, 515.
27 A. Borras, M. Macias-Montero, P. Romero-Gomez and A. R. Gonzalez-Elipe, *J. Phys. D: Appl. Phys.*, 2011, **44**, 174016.
28 W. Baumeister, R. Grimm and J. Walz, *Trends Cell Biol.*, 1999, **9**, 81.
29 P. A. Midgley, M. Weyland and H. Stegmann, *Advanced Tomographic Methods in Materials Research and Engineering*, ed. J. Banhart, OUP, Oxford, United Kingdom, 2007, pp. 335–373.
30 C. Kubel, A. Voigt, R. Schoenmakers, M. Otten, D. Su, T. C. Lee, A. Carlsson and J. Bradley, *Microsc. Microanal.*, 2005, **11**, 378.
31 P. A. Midgley and M. Weyland, *Ultramicroscopy*, 2003, **96**, 413.
32 P. A. Midgley, M. Weyland, J. M. Thomas and B. F. G. Johnson, *Chem. Commun.*, 2001, **18**, 907.
33 C. N. R. Rao, F. L. Deepak, G. Gundiahn and A. Govindaraj, *Prog. Solid State Chem.*, 2003, **31**, 5.
34 N. S. Ramgir, K. Subanna, Y. Yang, R. Grimm, R. Michiels and M. Zacharias, *J. Phys. Chem. C*, 2010, **114**, 10323.
35 V. G. Dubrovskii, G. E. Cirlin, N. V. Sibirev, F. Jabeen, J. C. Harmand and P. Werner, *Nano Lett.*, 2011, **11**, 1247.
36 P. Romero-Gomez, J. Toudert, J. R. Sanchez-Valencia, A. Borras, A. Barranco and A. R. Gonzalez-Elipe, *J. Phys. Chem. C*, 2010, **114**, 290932.
37 I. Levchenko, K. Ostrikov, M. Keidar and S. Xu, *Appl. Phys. Lett.*, 2006, **89**, 033109.
38 G. Z. Xing, X. S. Fang, Z. Zhang, D. D. Wang, X. Huang, J. Guo, L. Liao, Z. Zheng, H. R. Xu, T. Yu, Z. X. Shen, C. H. A. Huan, T. C. Sum, H. Zhang and T. Wu, *Nanotechnology*, 2010, **21**, 255701.
39 A. Lafuma and D. Quere, *Nat. Mater.*, 2003, **2**, 457.
40 A. Borras, P. Groening, J. R. Sanchez-Valencia, A. Barranco, J. P. Espinos and A. R. Gonzalez-Elipe, *Langmuir*, 2010, **26**, 1487.
41 A. Borras and A. R. Gonzalez-Elipe, *Langmuir*, 2010, **26**, 15875.
42 V. Rico, C. Lopez, A. Borras, J. P. Espinos and A. R. Gonzalez-Elipe, *Sol. Energy Mater. Sol. Cells*, 2006, **90**, 2944.
43 P. Romero-Gomez, S. Hamad, J. C. Gonzalez, A. Barranco, J. P. Espinos, J. Cotrino and A. R. Gonzalez-Elipe, *J. Phys. Chem. C*, 2010, **114**, 22546.
44 R. Georgekutty, M. K. Seery and S. C. Pillai, *J. Phys. Chem. C*, 2008, **112**, 13563.
45 M. K. Seery, R. george, P. Floris and S. C. pillai, *J. Photochem. Photobiol., A*, 2007, **189**, 258.
46 R. Wang, N. Sakai, A. Fujishima, T. Watanabe and K. Hashimoto, *J. Phys. Chem. B*, 1999, **103**, 2188.

